J. Fluid Mech. (2021), *vol*. 917, A43, doi:10.1017/jfm.2021.303

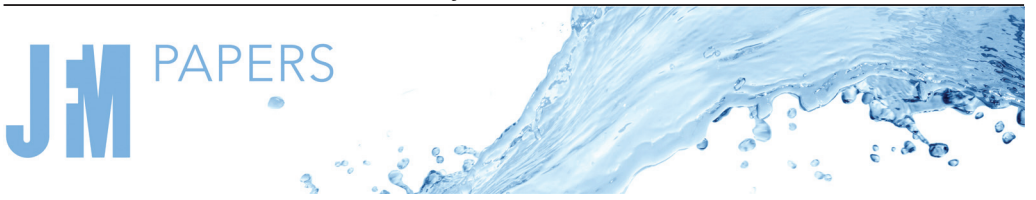

Transient dynamics of accelerating turbulent pipe flow

Byron Guerrero[1],†, **Martin F. Lambert**[2] **and Rey C. Chin**[1]

[1]School of Mechanical Engineering, University of Adelaide, Adelaide, South Australia 5005

[2]School of Civil, Environmental and Mining Engineering, University of Adelaide, Adelaide, South Australia 5005

(Received 1 December 2020; revised 21 February 2021; accepted 30 March 2021)

The transient dynamics of accelerating turbulent pipe flow has been examined using direct numerical simulation (DNS) data sets with a high spatiotemporal resolution, starting from low and moderate Reynolds numbers. The time-dependent evolution of the mean flow dynamics reveals that internal flows, during and after a rapid increase in the flow rate, experience four unambiguous transient stages: inertial, pre-transition, transition and core relaxation before they reach their final steady-state. The first stage is characterised by a rapid and substantial increment in the viscous forces within the viscous sublayer, together with the frozen behaviour of the existing turbulent eddies. The pre-transitional stage reveals a weak response of the turbulent inertia within the near-wall region, together with a rapid reduction in the viscous forces. At the third stage, termed transition, balanced growth in the magnitude of both the turbulent and the viscous forces within $y^{+0} \lesssim 50$ is observed. The final stage, referred to as core relaxation, shows a quasi-steady behaviour at $y^{+0} < 50$ and reveals the slow propagation of turbulence from the near-wall region into the wake region. A decomposition of the skin friction coefficient (C_f), using an FIK identity suitable for unsteady pipe flow, shows a progressive increment in the turbulent contribution during the core-relaxation period. Simultaneously, the unsteady contribution decreases proportionally, maintaining a plateau in C_f. The principal mechanism responsible for this slow regeneration in the wake is a temporal turbulence stratification at the inner region of the flow, together with a quiescent core, which maintains geometric coherence across extensive periods.

Key words: pipe flow, turbulence simulation, turbulent transition

† Email address for correspondence: byron.guerrerohinojosa@adelaide.edu.au

1. Introduction

Turbulent pipe flows are some of the most common flows found in daily applications. Although steady turbulent pipe flows have been studied extensively, these flows are seldom steady in most engineering applications. For instance, fluid supply pipe networks are usually connected to pumps and automatic/manual control valves, which modulate the flow rate continuously to fulfil the demands of a particular process. In these flows, it is possible to appreciate some physical behaviours that are not evident in steady turbulent flows.

Because transient turbulent pipe flows have received less attention than the steady case, the present investigation attempts to understand the dynamics of accelerating turbulent pipe flows, following a rapid ramp-up increment in the flow rate, in more detail from a fundamental perspective. To this end, a series of direct numerical simulation (DNS) data sets with a high spatiotemporal resolution have been used.

1.1. *Uniformly accelerating flows*

1.1.1. *A delayed response in turbulence*

A fascinating feature found in accelerating flows is that for a quick ramp-up increment in the flow rate of an initially turbulent flow, the 'new' turbulence scales do not develop at the same pace as the increment in the bulk velocity of the fluid. The pioneering study conducted by Maruyama, Kuribayashi & Mizushina (1976) on a step-wise accelerating turbulent pipe flow reported a delayed response in turbulence. Their study showed that turbulence initially regenerates near the wall and subsequently propagates in the wall-normal direction towards the pipe centreline. An experimental investigation conducted by Greenblatt & Moss (1999) during the flow excursion of a rapidly accelerating pipe flow at a high Reynolds number (Re) reported that during the early period ($t \leqslant 0.1$ s) of acceleration, the streamwise turbulence intensity at the near-wall region decreases, which provides hints about a possible turbulence suppression during a short time scale. Nevertheless, the same study showed that after $t > 0.1$ s, the turbulence fluctuations increased in intensity at $y^+ \approx 14$, while the turbulence response at the overlap and at the outer region of the flow remained unchanged. He & Jackson (2000) explored simultaneous measurements using a two-component laser Doppler anemometer (LDA), which resulted in the first three-dimensional study of accelerating flows starting from low Reynolds numbers at relatively low acceleration rates. The investigation mentioned above identified three delays associated with turbulence generation, energy re-distribution and radial propagation of turbulence. More recently, Jung & Chung (2012) tried to replicate and extend the study conducted by He & Jackson (2000) by using large-eddy simulation (LES) data sets. Similarly, they found that the turbulent response followed three stages: weak-time dependent, strong-time dependent and pseudo-steady, based on the same mechanisms reported in the former investigation. Greenblatt & Moss (2004) performed an experimental investigation of rapid temporal acceleration in turbulent pipe flows at high Reynolds numbers. Their study divided the transient behaviour of the pipe flow into three unsteady stages based on the coherence presented by the evolution of the displacement thickness (δ^*) and the shape factor (H) on a time scale normalised by the ramp rise time (T). The same study reported that turbulent scales respond first at the wall and propagate in the wall-normal direction within the inner region of the flow ($y^{+0} \lesssim 100$, where the '+' superscript denotes normalisation in viscous units and '0' refers to the initial steady-state of the flow). Surprisingly, a sudden increment in turbulence at $y^{+0} > 200$ was observed, which implied an early regeneration of the wake region. This effect was followed by a

constant response of turbulence at $y^{+0} \approx 130$, which showed that the wake region requires a long time to develop into the fully steady-state. Greenblatt & Moss (2004) argue that the contrasting results from previous experimental investigations could be attributed to differences in the initial Reynolds numbers, acceleration rates and spatial resolution in the wall-normal direction. Meanwhile, the reason why turbulence takes longer to propagate within the wake region has not yet been fully explained.

1.1.2. *Laminar perturbation velocity*

Further studies have shown that a critical attribute observed in accelerating internal wall-bounded flows after a rapid increase in the flow rate is the characteristic development of the velocity profile. The early experimental investigation conducted by Kurokawa & Morikawa (1986) explains that the velocity profile for an accelerating flow that starts from rest can be explained by the presence of a wide 'potential' core, together with a thin temporally developing boundary layer at the wall, which later evolves into a fully-developed turbulent profile. Likewise, more recent experimental (He & Jackson 2000) and numerical studies for transient flows starting from turbulent (Seddighi *et al.* 2013; He & Seddighi 2013, 2015) and laminar flow fields (Wu *et al.* 2015) have revealed that the evolution of the mean velocity profile of an internal flow at its early stages can be understood as the superposition of the initial turbulent mean velocity profile and a developing laminar boundary layer (Sundstrom & Cervantes 2017; Mathur *et al.* 2018). Consequently, this implies a reduction in the displacement thickness at the onset of the flow acceleration (Greenblatt & Moss 2004), superseded by a dramatic increase in the wall friction, which overshoots the steady-state values (Kurokawa & Morikawa 1986; Annus & Koppel 2011; He, Ariyaratne & Vardy 2011).

1.1.3. *Bypass-transition-like development*

Recent investigations, based on DNS (He & Seddighi 2013, 2015; Wu *et al.* 2015; He, Seddighi & He 2016) and experimental time series (Mathur *et al.* 2018), have also revealed that the transient behaviour in the mean velocity profile of rapidly accelerating flows leads to a time-dependent skin friction coefficient (C_f), whose behaviour has close similarities with the boundary-layer bypass transition. In contrast, if the flow rate of a turbulent base flow increases progressively, the bypass-transition-like behaviour is no longer observed (Jung & Kim 2017). The study conducted by He & Seddighi (2013) analysed the flow kinematics of accelerating channel flow at low Re in detail and suggested that the transitional process of the flow follows three stages: pre-transition, transition and fully turbulent. The pre-transition stage has been characterised as a period of 'buffeted laminar' behaviour, where the streamwise fluctuations respond progressively at the near-wall region, and the other two orthogonal turbulent components remain almost unchanged from the initial turbulent state. The end of the pre-transition (onset of transition) is specified as the instant when C_f reaches its minimum (He & Seddighi 2015). Subsequently, the transitional stage is denoted as a period where the wall friction recovers (Mathur *et al.* 2018) and new turbulent spots are generated, followed by propagation of the newly-formed turbulent structures in the wall-normal direction. During this stage, a difference has been found between the channel and pipe flow behaviour, mainly in the development of the core, where a faster turbulent response was found for the pipe flow case (He *et al.* 2016). Lastly, a fully-turbulent state is reached when the flow statistics are time invariant (He & Seddighi 2013). According to Mathur *et al.* (2018), the fully turbulent stage coincides with the first peak reached by C_f after the transition stage.

1.2. *Motivation*

The studies mentioned previously have provided significant contributions regarding the physics related to temporally-accelerated turbulent internal flows. Nevertheless, open questions remain related to these unsteady flows. To our knowledge, the extant literature has not yet offered a clear consensus and a robust method of identifying the temporal stages experienced by a rapidly-accelerating turbulent, internal, wall-bounded flow. Indeed, at least three different criteria have been presented (Greenblatt & Moss 2004; Jung & Chung 2012; He & Seddighi 2013) to distinguish the different stages concerning the temporal evolution of accelerating internal flows. The previous investigations have approached this based on the temporal evolution of basic quantities (e.g. δ^*, H, C_f) and the flow kinematics. Finally, most of the numerical simulations regarding accelerating channel and pipe flow have relied on turbulent base flows at low friction Reynolds numbers, typically $Re_\tau \approx 180$. Note that the friction Reynolds number is defined as $Re_\tau = u_\tau R/\nu$, where R is the pipe radius, ν is the kinematic viscosity of the fluid and u_τ is the friction velocity $u_\tau = \sqrt{\tau_w/\rho}$ with τ_w the mean wall shear stress and ρ the fluid density.

The radial propagation delay of turbulence observed in early experimental studies (Maruyama *et al.* 1976; He & Jackson 2000) has been confirmed in recent numerical studies (Jung & Chung 2012; He & Seddighi 2013). Nevertheless, it should be noted that those studies have used turbulent initial fields at low initial Re. Additionally, experiments with accelerating flows at high Reynolds numbers (Greenblatt & Moss 2004) have presented contrasting results regarding how turbulence regenerates in the wall-normal position. Another aspect noted in the evolution of an accelerating flow is a slow reconstitution in the wake region of the flow (Greenblatt & Moss 2004; He & Seddighi 2013). However, it is still unclear why the core of the flow requires such a large time scale to relax towards the final steady-state.

Thus, the present investigation aims to consolidate and extend the studies mentioned above by examining the different stages experienced by a turbulent flow after a rapid increase in the flow rate, based on the temporal evolution of the dynamic components in the mean momentum balance, from a novel DNS database with a high spatiotemporal resolution ranging from low to moderate initial Reynolds numbers. After using different methodologies, it is demonstrated that the transient behaviour of a turbulent pipe flow following a rapid temporal acceleration can be defined in four clear and unambiguous stages. By extending the works of Greenblatt & Moss (2004) and He & Seddighi (2013, 2015), the four transitional stages have been named inertial, pre-transition, transition and core relaxation. Furthermore, we present an alternative expression of the FIK identity suitable to decompose C_f for transient pipe flows. This approach sheds light on how the different dynamic components of the momentum balance contribute to the skin friction coefficient during the transient process. The results reveal that a plateau in the skin friction coefficient is not necessarily an appropriate indication from which to determine the onset of the final steady-state in the flow. Furthermore, the slow regeneration of turbulence in the wake region of the flow is explained using the method proposed by Adrian, Meinhart & Tomkins (2000), where we analyse the transient behaviour of the largest uniform momentum zone (UMZ) of the flow, namely, the core region during the last transitional stage.

Finally, an advanced understanding of the dynamics of unsteady turbulent pipe flow is provided in this investigation. Together with the studies referred throughout this paper, the present results can be used as the foundation for developing more precise unsteady friction models (Vardy & Brown 2003; Dey & Lambert 2005; Vardy *et al.* 2015).

Case	$Re_{\tau,0}$	$Re_{\tau,1}$	Δt^{+0}_{ramp}	Δt^{+0}_{samp}	δ	γ	Δz^{+1}	$\Delta R\theta^{+1}$	Δy^{+1}_{wall}	Δy^{+1}_{core}	Gridpoints
TP1	500	670	11.8	0.6	0.035	34.36	7.4	6.3	0.05	7.5	328×10^6
TP2	171	320	23.5	1.0	0.041	14.37	7.8	6.4	0.03	7.9	49×10^6
TP3	171	340	47.0	1.0	0.025	8.56	8.5	7.0	0.04	8.2	49×10^6
TP4	171	415	23.5	1.0	0.078	27.48	10.1	8.3	0.04	8.2	49×10^6

Table 1. Computational parameters used in the numerical simulations. The '+' superscript denotes normalisation in viscous units, and the '0' and '1' indices denote the initial and final steady-states. The subscripts '*ramp*' and '*samp*' refer to the acceleration time and the sampling time intervals at which three-dimensional flow realisations have been stored, respectively. The variables $\delta = [\mathrm{d}U_b/\mathrm{d}t\ \nu/(U_{b0}u^2_{\tau 0})]$ and $\gamma = [\mathrm{d}U_b/\mathrm{d}t\ D/(U_{b0}u_{\tau 0})]$ are the dimensionless ramp-rate parameters proposed by He & Jackson (2000). The high values of γ (i.e. $\gamma \gg 1$) indicate that, in all cases, the flow behaves as an unsteady turbulent flow and should present large deviations concerning the pseudo-steady case.

2. Methodology

2.1. *Numerical details*

The present data were collected using the spectral element solver Nek5000 (Fischer, Lottes & Kerkemeier 2019). The numerical schemes used to conduct the current DNS have been explained in detail in Guerrero, Lambert & Chin (2020). In all the cases investigated herein, the simulations ran for at least seven turnovers (TU_b/L_z) on a periodic domain with a streamwise length $L_z = 8\pi R$ before the flow was accelerated. This approach ensured statistically steady turbulence at the initial Reynolds number before accelerating the flow and helped to suppress any numerical influences of the initial perturbations in the flow fields (Chin 2011). Subsequently, an increase in the flow rate was applied in cases TP1 to TP3 (see table 1) by setting a linear increment in the bulk velocity, except for case TP4, where the flow was accelerated by imposing a step-up increase in the magnitude of the pressure gradient. It should be mentioned that case TP4 was conducted to determine if different methods of imposing the acceleration would make a difference to the results. The results (in § 3.1) show that both methods used to accelerate the flow are valid. The simulations were run three times in all cases, starting from uncorrelated turbulent fields to provide convergent statistics. All the study cases showed similar features in the statistical results and the temporal flow development, further explained and analysed in § 3. The main parameters, such as the initial and final Reynolds numbers, the ramping time and the grid resolution, used in all the simulations performed for this investigation are briefly summarised in table 1.

The notation that defines the cylindrical coordinate system used in this study is r, θ and z in the radial, azimuthal and streamwise directions, respectively. The wall-normal direction is defined as $y = R - r$, where R is the pipe radius. The velocity components are U_z, U_θ and $U_y = -U_r$ with fluctuating components u_z, u_θ and $u_y = -u_r$. The superscript '+' stands for inner normalization in viscous units, where $\delta_\nu = \nu/u_\tau$ is the viscous length, ν represents the kinematic viscosity and u_τ is the friction velocity. Because this investigation focuses on the transient behaviour of accelerating turbulent pipe flows between two different Reynolds numbers, the numbers '0' and '1' are used to denote the initial and the final steady-states, respectively.

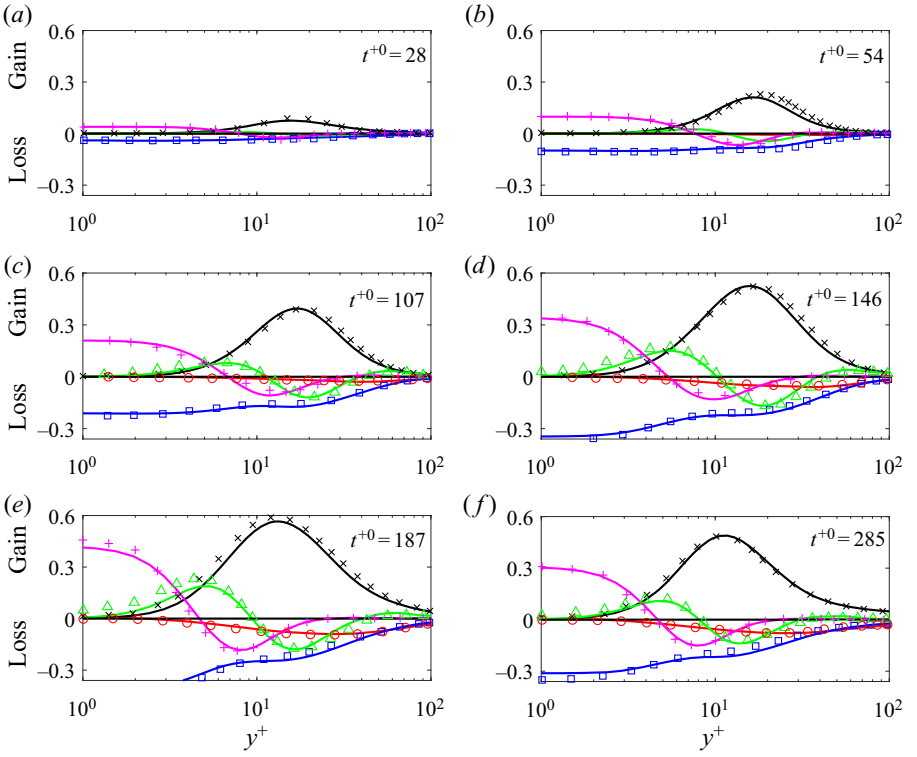

Figure 1. The $u_z u_z$ budget terms of (solid) present case TP2, (symbols) He & Seddighi (2013), (black) production, (blue) viscous dissipation, (green) turbulent transport, (magenta) viscous diffusion and (red) pressure strain. The budgets have been computed during the (*a–c*) pre-transition and (*d–f*) transitional stages.

2.2. *Validation*

Herein we validate the transient behaviour of the present DNS data of case TP2 ($Re_\tau \approx 170$–320) with the results from the detailed DNS study of transient channel flow by He & Seddighi (2013), which has been conducted at similar Reynolds numbers. Fully-developed resolved turbulent fields from Guerrero *et al.* (2020) have been used as the initial steady-state before the flow excursion. It should also be mentioned that the benchmark data were computed for a different geometry (channel flow), after a step-wise increment in the flow rate, and slightly different initial and final Reynolds numbers ($Re_\tau \approx$ 180–420).

To ensure that not only the velocity and pressure fields are correct, but also the velocity gradient tensor is accurate, we compare the $u_z u_z$ budget terms of case TP2, normalised in viscous units by the instantaneous values of u_τ^4/ν. Figure 1 compares the present results with the benchmark data during the pre-transition (*a–c*) and transition stages (*d–f*). Although both numerical simulations have been conducted for different geometries, initial and final Re_τ, and acceleration rates, it should be noted that high-order statistics, such as the $u_z u_z$ budgets, exhibit a similar behaviour and good collapse during the transient stages. The small dissimilarities between the present and the benchmark data were attributed to the differences mentioned previously and different numerical methods, mesh resolution and domain length. Hence, these results allow us to be confident with the validity of the DNS data used in this investigation.

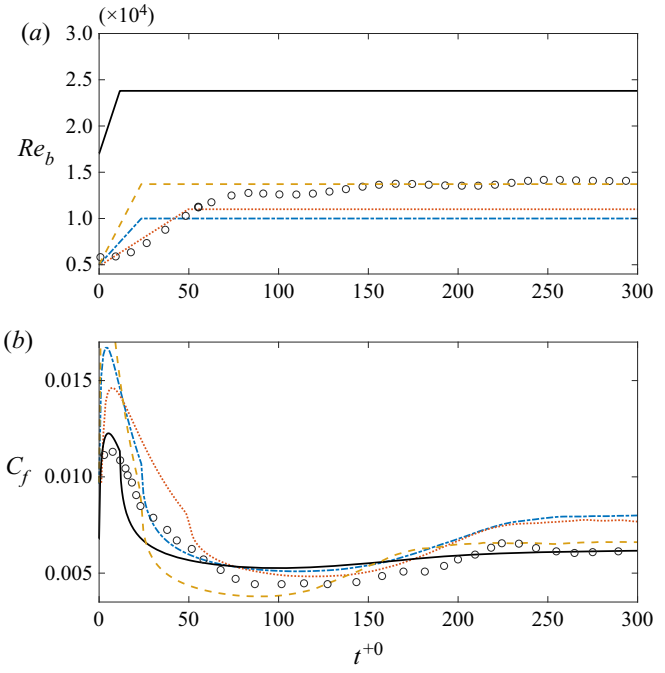

Figure 2. (*a*) Temporal development of the bulk Reynolds number Re_b on a time domain scaled by the initial viscous units t^{+0}. (*b*) Temporal evolution of the friction coefficient C_f. The notation of the present cases are (——) TP1, (– · –) TP2, (· · · · · ·) TP3, (– – –) TP4. The symbols (○) are the PIV data by Mathur (2016).

3. Results and discussion

3.1. *Skin friction coefficient*

Before analysing the flow dynamics relevant to accelerating flows, we show the behaviour in the skin friction coefficient ($C_f = 2u_\tau^2/U_b^2$), which has been used as an indicator to identify the different transitional stages experienced by a rapidly accelerating turbulent flow (He & Seddighi 2013; Mathur *et al.* 2018). Figure 2(*a*) shows the linear increment in the bulk Reynolds number ($Re_b = 2U_bR/\nu$) of the cases analysed in the present study on a time-domain normalised in terms the initial viscous units ($t^{+0} = t\, u_{\tau,0}^2/\nu$). The present case TP3 (orange) exhibits a similar acceleration rate as the particle image velocimetry (PIV) data collected by Mathur (2016) (symbols). Figure 2(*b*), displays the behaviour of the ensemble-averaged skin friction coefficient. The temporal evolution of the C_f regarding the current cases TP1–TP4 also exhibits similarities to the spatial development of the boundary layer bypass transition identified by He & Seddighi (2013). Furthermore, similar characteristics have been observed in previous DNS studies related to the laminar to turbulent transition of pipe flow with a plug inflow perturbation (Wu *et al.* 2015).

A careful examination of the skin friction, displayed in figure 2(*b*), reveals that at the onset of the flow excursion, there exists a rapid increment in C_f resulting from a large nonlinear increment in the wall shear stress τ_w, whose magnitude grows faster and is not proportional with the temporal increment of the flow rate. This implies that the viscous effects have an essential role within the viscous sublayer during the early stage of the flow excursion. This short stage at which the viscous forces are dominant near the wall has been named inertial throughout the present investigation. Then, C_f reaches a maximum

at $t^{+0} \approx 10$. This shows that the lapse required in the viscous stresses at the wall to reach a peak seems to scale in the initial viscous units rather than the ramp-up interval (Greenblatt & Moss 2004). In all the current cases, it is observed that C_f presents a slow decay at $t^{+0} \gtrsim 10$ and before the ramp-up increase in the flow rate ceases, which shows a wall-normal diffusion of the viscous forces, as further explained in the later sections (Note that this short stage has not been characterised by He & Seddighi (2013, 2015) because they conducted step increments in the flow rate, where this stage might become extremely short.). When the bulk velocity becomes constant at its highest value, C_f decays rapidly and afterwards reaches a minimum; He & Seddighi (2013) designated this stage as pre-transition. As a minimum in the friction coefficient is attained, instabilities grow, turbulence is regenerated and C_f recovers. This stage, where a significant increment in the turbulence kinetic energy (TKE) is observed, is known as transition. According to Mathur *et al.* (2018), after the skin friction recovery, a peak is reached by C_f and the flow becomes fully-turbulent, which is subsequently observed in the constant behaviour of the friction coefficient. Nevertheless, previous experimental (Greenblatt & Moss 2004) and numerical studies (He & Seddighi 2013) revealed that the wake region of the flow might require large time scales before it regenerates completely. Hence, the plateau attained by the mean skin friction coefficient might not be a clear indicator to determine the moment at which the flow has fully developed. Throughout this investigation, the period at which turbulence shows a quasi-steady-state near the wall, but the wake region is still developing, will be designated as core relaxation. To extend and complement the studies mentioned above, in the following sections, the time evolution of the turbulent eddies, the Reynolds and viscous shear stresses, the mean flow dynamics and the momentum re-distribution of the flow are analysed to provide a qualitative and a quantitative relation between the flow dynamics and the frictional drag, especially during the inertial and the core-relaxation periods.

3.2. *Flow visualisation*

3.2.1. *Vortical structures*

Figure 3 depicts the temporal evolution and the transient process of the vortical structures for case TP2, because the vortical structures can be visualised with more clarity at lower *Re*. The vortices have been identified using the λ_2 criterion (Jeong & Hussain 1995) and are plotted at a level $\lambda_2^+ = -0.5$. In figure 3(*a*), it is observed that during the inertial stage, the λ_2 structures advect with the mean flow without showing a major evolution in its topology. Both snapshots presented in figure 3(*a*) have been taken during the flow excursion. This 'frozen' behaviour of turbulence is consistent with previous experimental works (Maruyama *et al.* 1976; Greenblatt & Moss 1999). In the lower-left corner of figure 3(*a*), an $r-\theta$ view of the pipe flow at $t^{+0} = 10$ is presented, where it is observed that there exist vortical structures from the wall up to $y/R \approx 0.6$.

During the pre-transition (figure 3*b*), it is observed that oblique and quasi-streamwise vortices are stretched in the streamwise direction, and, as time progresses, they become more aligned in the z-direction. The stretched vortex filaments induce wall-normal motions, which in turn re-distribute momentum and generate elongated streamwise velocity streaks (He & Seddighi 2013), distributed more or less evenly in the azimuthal direction. The behaviour of the velocity streaks is explained in more detail in § 3.2.2.

Some elongated streaks exhibit a sinuous pattern by the end of the pre-transition/onset of transition. Subsequently, nonlinear secondary instabilities are engendered and, as they grow, individual patches of smaller turbulent eddies emerge within the flow. These turbulent spots, populated by hairpin-like structures, are observed at the onset of transition,

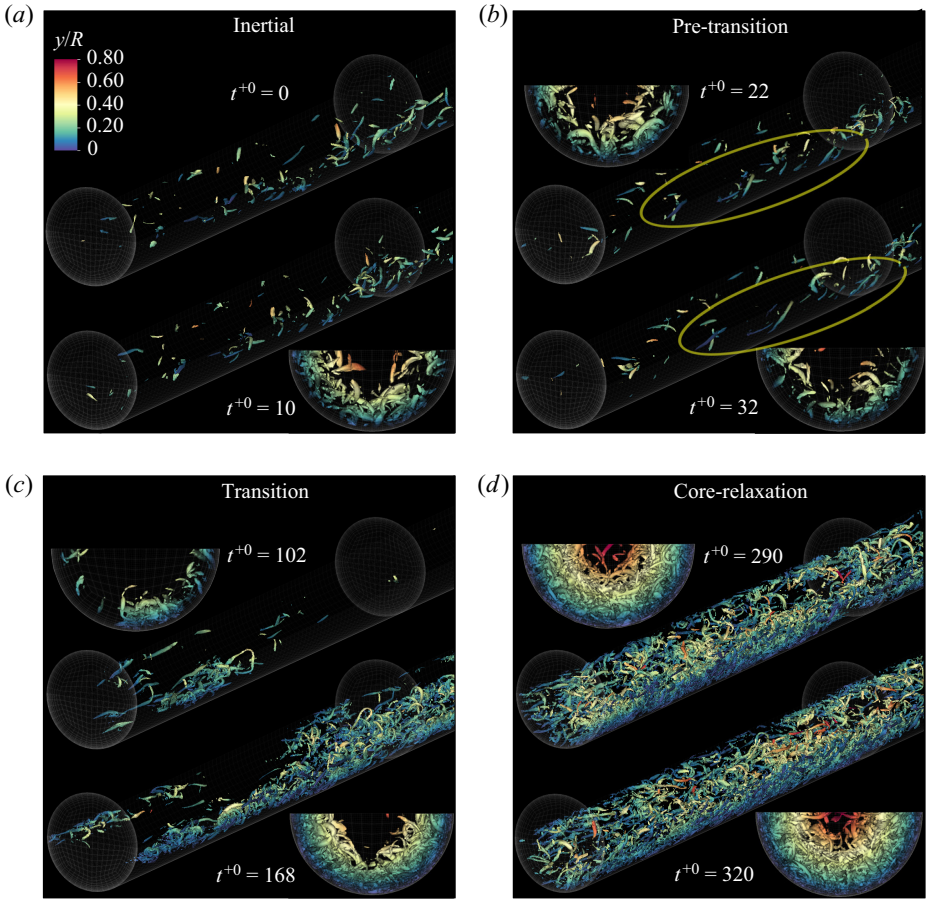

Figure 3. Temporal evolution of the vortical structures for case TP2 based on the λ_2 criterion. The isosurfaces are coloured by the wall-normal distance y/R. (*a*) inertial stage, (*b*) pre-transition, (*c*) transition and (*d*) core relaxation. The yellow ellipses in (*b*), during the pre-transition stage, highlight a region where several quasi-streamwise vortices are stretched between two consecutive snapshots. Note that in all the snapshots, only the lower half of the pipe is displayed for clarity.

which occurs in the vicinity of a minimum C_f. It should be stated that the turbulence proliferation mechanisms, observed at the early transition, exhibit strong similarities with the transition from laminar to turbulent motion in pipe flow (Avila *et al.* 2011; Wu *et al.* 2015). The turbulent spots that characterise the onset of transition are exhibited in figure 3(*c*) at $t^{+0} = 102$. It should be mentioned that the leading edge of the turbulent spots seems to move with the mean flow without affecting the upstream base flow. As time progresses, new turbulent eddies emerge at the rear ends of the turbulent spots. This shows that turbulent spots are particularly unstable at their trailing ends and provides further evidence of the observations made by Hof *et al.* (2010). The isometric and the $r - \theta$ views obtained at $t^{+0} = 102$ and 168 respectively show that turbulent spots grow and merge during the transition period. The regeneration of turbulent structures produces a higher mean skin friction, and therefore, it explains the recovery of C_f during this stage. Turbulent eddies propagate at a slower pace in the wall-normal direction (Maruyama *et al.* 1976). The larger turbulent spot captured at $t^{+0} = 168$ is highly populated by hairpin structures whose trailing legs are attached to the wall and show similarities with the hairpin forests studied by Head & Bandyopadhyay (1981) and Perry & Chong (1982).

The turbulence response during the last stage, namely core relaxation, is observed in the vortical structures depicted in figure 3(*d*). During this period, there is a dense population of turbulent eddies along the pipe from the wall up to a wall-normal location $y/R \approx 0.5$, and there are very few vortical structures at $y/R > 0.5$, as observed in the snapshot taken at $t^{+0} = 290$. As time progresses, the λ_2 structures continue to propagate towards the pipe centreline at a slow pace. The mechanisms associated with this slow regeneration of turbulence in the wake region during the last transient stage are further examined in § 3.7.

3.2.2. *Velocity streaks*

Here, the structural behaviour of the streamwise velocity streaks at the near-wall region during the four transient stages is analysed. The left column of figure 4 exhibits the two-point correlation of the streamwise velocity fluctuations $R_{u_z u_z}$ for case TP2 over a wall-parallel plane located at $y^{+0} \approx 7$, which provides a statistic characterisation of the average half-length of the streaks. The right column in figure 4 displays instantaneous visualisations of the streamwise velocity streaks at the same wall-normal position. The flow visualisations (figure 4*e*,*h*) show good agreement with earlier investigations (He & Seddighi 2013; He *et al.* 2016; Mathur *et al.* 2018). Figure 4(*a*) exhibits an unchanged behaviour of the streaks during the inertial stage and reveals an average half-length of $\Delta z^{+0} \approx 671$ at this wall-normal position. This unchanged behaviour during the first stage is consistent with the 'frozen' turbulence observed during the first instances of the flow excursion (Maruyama *et al.* 1976; He & Jackson 2000; Greenblatt & Moss 1999, 2004).

The results observed in figure 4(*b*), through the pre-transition period, suggest an elongation of the near-wall velocity streaks. At the end of this stage, the streaks reach an average half-length of $\Delta z^{+0} \approx 1080$ and agree well with the length scales reported by He *et al.* (2016) during the late pre-transition. Also, figure 4(*f*) provides a qualitative insight into this behaviour. It should be mentioned that the elongation of the streaks is consistent with the stretching of the quasi-streamwise vortices discussed previously and observed in figure 3(*b*). As near-wall quasi streamwise vortices are stretched during this stage, the magnitude of the vorticity vector increases to preserve the angular momentum, which agrees with the growth of the streamwise stress $\langle u_z u_z \rangle$ within the near-wall region during this stage (He & Seddighi 2013).

Figure 4(*c*), associated with the transitional process, exhibits a progressive reduction in the length scale of the streaks. These observations are consistent with the development of nonlinear secondary instabilities (hairpin-like vortical structures) observed at the onset of transition. The secondary instabilities lead to the breakdown process of the streaks, which initially looks like isolated spots, as observed in figure 4(*g*). As time progresses, sinuous and varicose breakdown processes continue occurring with increasing frequency. Consequently, the turbulent spots grow and merge within the inner region of the flow.

Finally, as the core-relaxation process takes place (figure 4*d*,*h*), only minor changes are observed in $R_{u_z u_z}$ at this wall-normal position as, during this stage, turbulence propagates from the wall towards the pipe centreline. By the end of the core relaxation, the average streak has an average half-length of $\Delta z^{+0} \approx 420$. This reduction in the length scale is consistent with the increase in the Reynolds number imposed in case TP2.

3.3. *Viscous and Reynolds shear stresses*

Throughout the rest of this paper, the four transient stages of accelerating pipe flow are explained from a statistical point of view, based on case TP1. The data from this case have

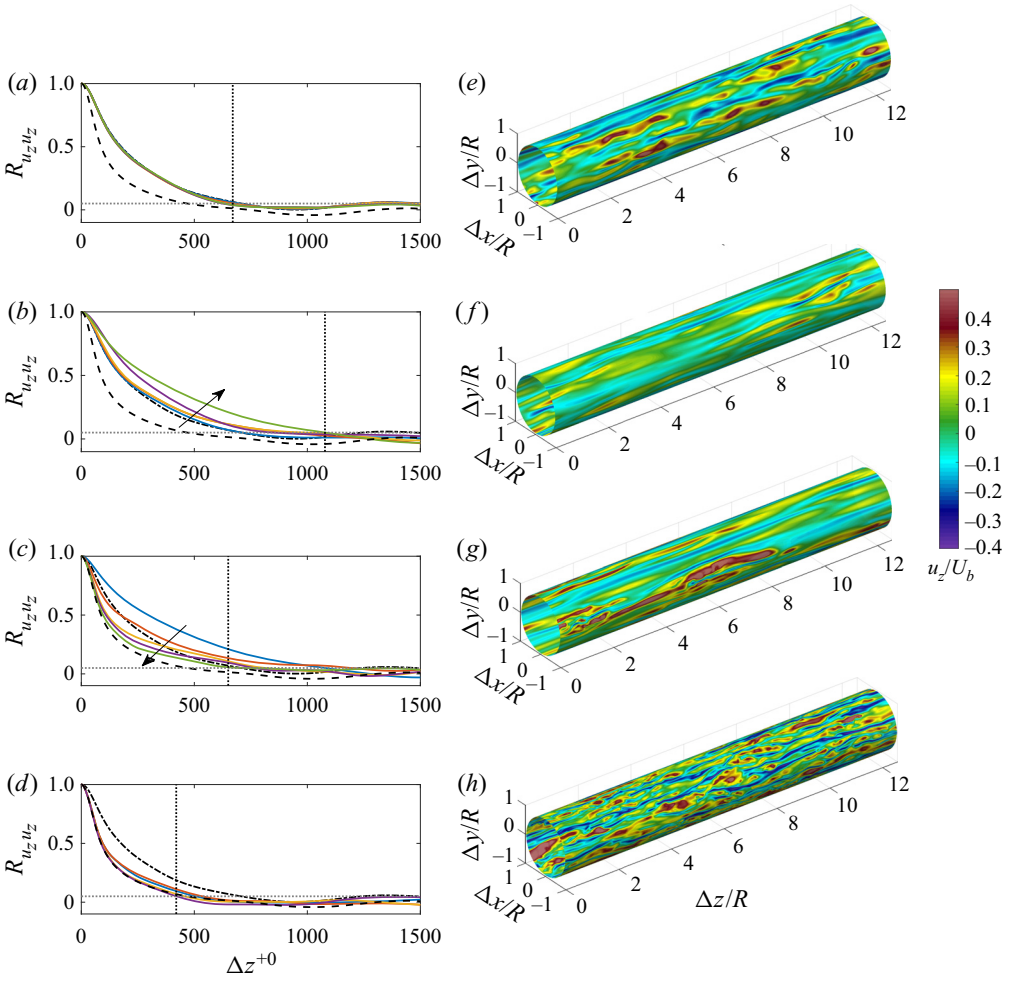

Figure 4. Time dependency of the streamwise velocity fluctuation structures at $y^{+0} \approx 7$ for case TP2. The left column exhibits the streamwise two-point correlation $R_{u_zu_z}$ at $y^{+0} \approx 7$ during the four stages (*a*) inertial $0 \leqslant t^{+0} \lesssim 10$, (*b*) pre-transition $10 < t^{+0} \lesssim 100$, (*c*) transition $100 \lesssim t^{+0} \lesssim 250$ and (*d*) core relaxation $t^{+0} \gtrsim 250$. (– · –) Initial turbulent steady-state, (– – –) final steady-state. The arrows represent an increase in time. The intersection between the vertical and horizontal (· · · · · ·) lines show streamwise length of the positive correlated regions at $R_{u_zu_z} = 0.05$. For the colour legend, refer to figure 5. The right column shows the qualitative behaviour of the low-speed streaks at (*e*) $t^{+0} = 0$, (*f*) $t^{+0} = 32$, (*g*) $t^{+0} = 102$, (*h*) $t^{+0} = 290$.

been chosen as it was conducted at a moderately high initial Reynolds number $Re_\tau \approx 500$, and its dynamics also present clear four-layer behaviour (Wei *et al.* 2005), which is less likely to be observed at lower Reynolds numbers (Klewicki *et al.* 2012). It should be stated that the same analysis has been conducted for all the cases listed in table 1, where the same temporal evolution is observed during the transient process.

The temporal evolution of the Reynolds $\langle u_r u_z \rangle^{+0}$ and viscous $\langle \mathrm{d}U_z/\mathrm{d}y \rangle^{+0}$ shear stresses for case TP1 are depicted in figure 5 and shed light on the attributes of the four well-defined stages that characterise the transient behaviour of the flow. Note that the fluid increases its total kinetic energy owing to an increase in the flow rate, mainly during the inertial stage. It should also be mentioned that over the last two stages (i.e. transition and core

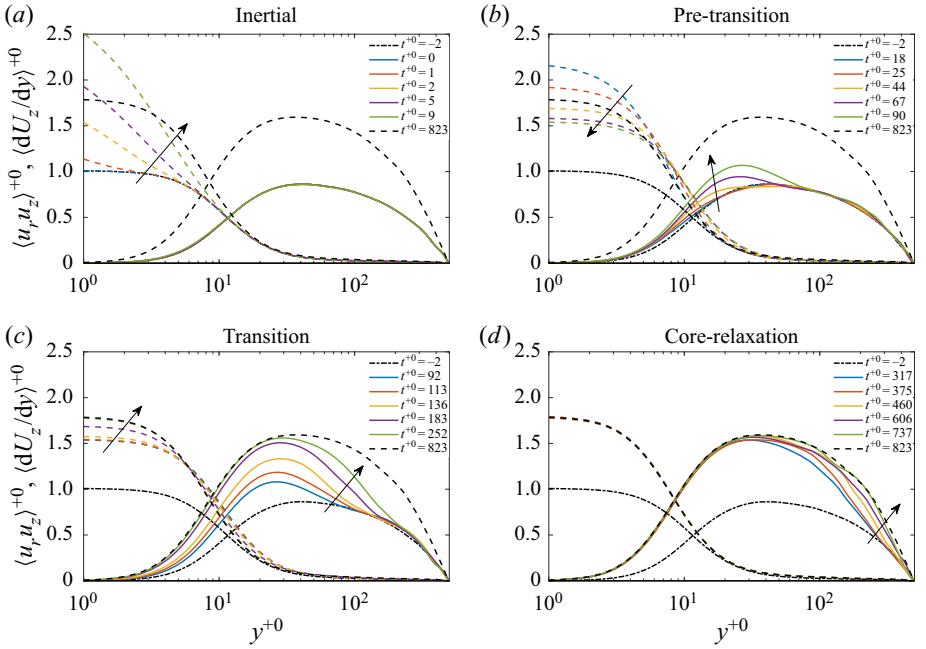

Figure 5. Time evolution of the Reynolds and the viscous shear stresses. $(- \cdot -)$ Initial turbulent steady-state, $(- - -)$ final steady-state, (solid) Reynolds shear stress and (dashed coloured) viscous shear stress. The arrows represent an increase in time.

relaxation), the flow does not present an increment of its total kinetic energy. However, its dynamics reveals an organised and time-dependent redistribution in momentum along the wall-normal direction.

Figure 5(*a*) reveals that during the first stage, the Reynolds stress remains almost unchanged. This implies the existence of a delay in the turbulence response, consistent with Maruyama *et al.* (1976) and He & Jackson (2000). Specifically, the turbulent base flow remains statistically unchanged during this short stage and acts as a convective perturbation, which triggers the instabilities needed to increase the turbulent energy throughout the subsequent stages to reach a final equilibrium state. Additionally, during this stage, the viscous stress exhibits a rapid increment in magnitude within the viscous sublayer, overshooting the value of its final steady-state, and its influence propagates in the wall-normal direction. The high shear produced at $y^{+0} < 10$ is generated owing to the superposition of a plug-like inflow on the initial turbulent flow. This plug inflow generates a small layer with high-velocity gradients, which subsequently develops as a time-dependent perturbation boundary layer (Mathur *et al.* 2018).

Figure 5(*b*) shows that the pre-transition stage ($10 \leqslant t^{+0} \leqslant 90$) is characterised by a weak growth of the Reynolds shear stress, which starts at the buffer region at $y^{+0} \approx 10$. This slight increase in the magnitude of the Reynolds shear stress is related to an energy growth in the streamwise Reynolds stress $\langle u_z u_z \rangle$ (not shown here), which in turn is associated with the elongation of the streamwise velocity streaks located at the near-wall region, characteristic of the pre-transitional phase (He & Seddighi 2013; He *et al.* 2016). By the end of the pre-transition ($t^{+0} \approx 90$), a sudden turbulence response is observed at $y^{+0} \approx 200$, which agrees with the experimental observations by Greenblatt & Moss (2004). However, the Reynolds shear stress behaviour throughout the two final stages

suggests that radial propagation is the main mechanism by which turbulence penetrates the core of the flow (Maruyama *et al.* 1976; He & Jackson 2000). In the same figure, it is observed that the magnitude of the viscous stress decays at the viscous sublayer, undershooting the value of its final steady-state. The present results also reveal that although the magnitude of the viscous stress decays at the viscous sublayer during this stage, it slowly grows at the buffer region, which provides evidence for a radial propagation of the viscous forces, as discussed further in § 3.4.

The transition stage shown in figure 5(*c*) reveals a faster growth of $\langle u_r u_z \rangle^+$ at $y^{+0} < 50$ compared with the pre-transition stage. Additionally, turbulence is temporally propagated in the wall-normal direction, consistent with Maruyama *et al.* (1976) and He & Jackson (2000). Interestingly, at the wake region, the turbulent response remains nearly unchanged after the sudden growth observed at the end of the pre-transition stage ($t^{+0} \approx 90$), where an early response at $y^{+0} \approx 200$ was observed. This behaviour suggests another mechanism that delays the turbulent response associated with the more quiescent large-scales of motion (LSM) that exist at the core of the flow. In contrast, the magnitude of the viscous stress increases at the viscous sublayer at a lower rate than the Reynolds shear stress and decreases within the buffer region. This behaviour in the viscous/Reynolds stresses implies that the new buffer layer vortical structures start accelerating the flow near the wall, reshaping the mean velocity profile towards its final steady-state, as will be discussed in § 3.4.

In figure 5(*d*), at $t^{+0} > 300$, it is possible to observe that the Reynolds shear stress is almost unchanged within $y^{+0} \lesssim 100$, which shows that the flow has reached a quasi-steady-state at the inner region. However, a significantly slow regeneration of turbulence at the core region is evinced, which implies a temporal stratification of turbulence between the inner and wake regions of the flow. Interestingly, similar behaviour, in terms of a limited turbulent penetration length in the wall-normal direction, was observed by Scotti & Piomelli (2001) for pulsating channel flows at high frequencies. However, an unchanged behaviour in $\langle \mathrm{d}U_z/\mathrm{d}y \rangle^{+0}$ can be observed, which suggests that the viscous stress has reached a steady state. These results reveal that the steady-state mean velocity profile for the higher (final) Reynolds number is reached first at the near-wall region because it is strongly influenced by the viscous effects and the buffer layer vortical structures, which are generated and propagated during the late pre-transition and transitional stages. However, the outer region takes longer to reach the final steady-state, as it relies on turbulence diffusion from regions with a high production of TKE (buffer region) towards the less productive locations (wake) and the more quiescent LSM located at the core of the pipe.

Finally, cases TP2, TP3 and TP4, which start at low Reynolds numbers, were analysed in the same form as case TP1. Similarly, the results (not shown here) revealed four stages with the same behaviour exhibited in figure 5. A difference between the low and the moderate *Re* cases was found during the core-relaxation stage. Strictly speaking, the core-relaxation period lasts for shorter durations ($\Delta t^{+0} \approx 50$) for cases TP2, TP3 and TP4 compared with case TP1, whose core relaxation is $\Delta t^{+0} \approx 500$. This behaviour reveals that the time scales required for new turbulence, generated near the wall, to penetrate the wake region might depend on the initial Reynolds number. The relatively thick near-wall region and the almost non-existent separation of scales of turbulent flows at low *Re* explain this difference in the time required to reconstitute the wake. However, a complete study on the *Re* dependence of the wake regeneration is beyond the scope of this investigation.

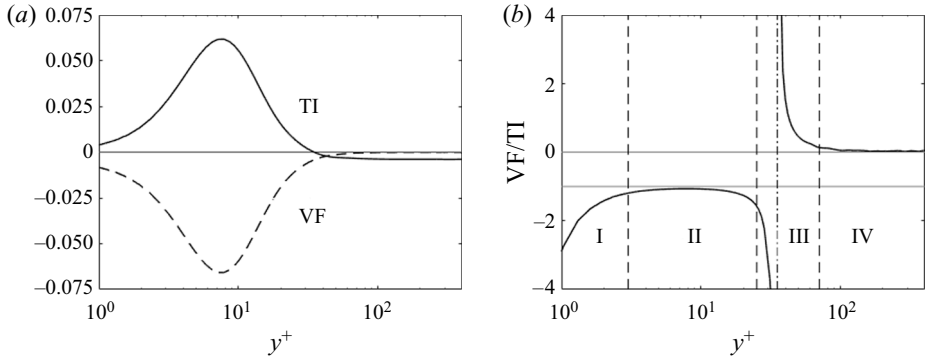

Figure 6. (*a*) Distribution of the mean TI and mean VF for the present DNS data at $Re_\tau \approx 500$. (*b*) The VF/TI ratio of pipe DNS at $Re_\tau \approx 500$, which shows a typical four-layer dynamic regime in a steady turbulent pipe flow. The line $- \cdot -$ shows the location of the zero crossing of TI.

3.4. *Dynamic behaviour of rapidly accelerating flows*

The mean streamwise momentum equation for an unsteady turbulent pipe flow, which is homogeneous in the z- and θ-directions in cylindrical coordinates, can be described as

$$\underbrace{\frac{\mathrm{d}\langle U_z\rangle}{\mathrm{d}t}}_{\mathrm{IF}} = \underbrace{-\frac{1}{\rho}\frac{\mathrm{d}p}{\mathrm{d}z}}_{\mathrm{PG}} + \underbrace{\frac{1}{r}\frac{\partial}{\partial r}\left(r\nu\frac{\partial\langle U_z\rangle}{\partial r}\right)}_{\mathrm{VF}} \underbrace{-\frac{1}{r}\frac{\partial}{\partial r}\left(r\langle u_r u_z\rangle\right)}_{\mathrm{TI}}. \tag{3.1}$$

Four physical mechanisms are represented in (3.1), which constitute Newton's second law applied to an infinitesimal fluid element in the streamwise direction. The term on the left-hand side is the unsteady behaviour (temporal acceleration) or the inertia force (IF) of the fluid. The first term on the right-hand side is the pressure gradient (PG). The last two terms at the right-hand side of (3.1) represent the viscous force (VF) and the turbulent inertia (TI). Figure 6(*a*) shows the distribution of the TI and the VF of case TP1, at the initial steady-state ($Re_\tau \approx 500$), before the flow excursion started. The VF (gradient of the viscous stress) acts as a sink term which decelerates the flow near the wall to fulfil the no-slip condition. In contrast, the TI acts as a momentum source within the near-wall region. Note that the turbulent inertia has a value of TI $= 0$ at the peak of the Reynolds stress, which indicates the onset of the logarithmic region (Wei *et al.* 2005; Klewicki *et al.* 2012; Chin *et al.* 2014) and becomes negative (momentum sink) at the overlap and wake regions. Physically, the TI accelerates the flow at the near-wall region and decelerates it at the outer layer, which leads to the well-known flatter mean velocity profile characteristic of internal wall-bounded flows.

The VF/TI ratio (viscous/Reynolds stress gradient) has proven to be a clear indicator of the predominant mean dynamics of canonical turbulent wall-bounded flows. The study conducted by Wei *et al.* (2005) revealed that the canonical flows follow a four-layer structure, where each layer is Reynolds-number-dependent and is characterized by having different internal dynamics. Figure 6(*b*) shows the VF/TI ratio of the present DNS data at $Re_\tau \approx 500$ and exhibits the force balance of the fluid elements in the wall-normal direction for a steady turbulent flow. The four layers have been divided in terms of the order of magnitude existing within them (Klewicki *et al.* 2012). Within layer I, the viscous forces are dominant ($|\mathrm{VF}| \gg |\mathrm{TI}|$). In layer II, there exists a balance between VF and TI ($|\mathrm{VF}| \approx |\mathrm{TI}|$). Layer III, where the zero-crossing of TI occurs, is characterised by

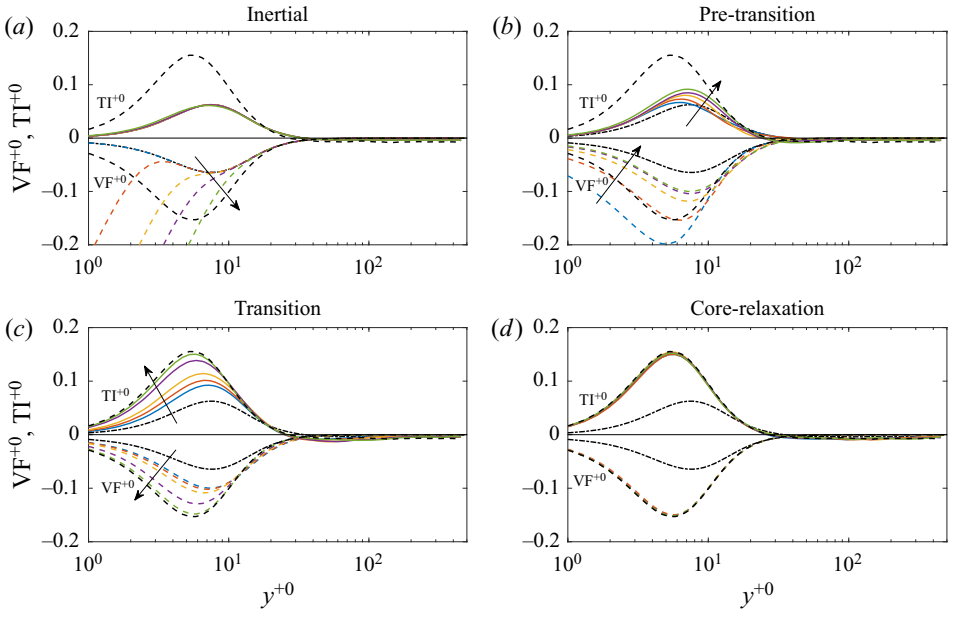

Figure 7. Time evolution of the turbulent inertia and the viscous force. (– · –) Initial turbulent steady-state, (– – –) final steady-state, (solid) turbulent inertia and (dashed) viscous force. The quantities have been normalised with initial viscous units by $u_{\tau,0}^3/\nu$. For the colour legend, refer to figure 5. The arrows represent an increase in time.

$|\mathrm{VF}| \gtrsim |\mathrm{TI}|$. Finally, in layer IV, VF becomes negligible compared with the magnitude of the turbulent force ($|\mathrm{VF}| \ll |\mathrm{TI}|$).

This section will focus on the behaviour of the turbulent inertia, viscous force and the VF/TI ratio to analyse in detail the momentum re-distribution during the transient period of case TP1. Figure 7(*a*) shows that during the inertial stage, the VF dramatically increases in magnitude at the wall and propagates in the wall-normal direction up to the buffer layer ($y^{+0} \lesssim 15$). This reveals that VF becomes an important momentum sink within the viscous sublayer, as the flow is accelerated to preserve the no-slip condition at the wall. As a result, high values of τ_w and a quick increment of C_f are observed at this stage. However, TI in figure 7(*a*) remains nearly unchanged, which provides further evidence that there exists a delay in the response of the turbulence when the flow is initially accelerated (Maruyama *et al.* 1976; He & Jackson 2000; He & Seddighi 2013).

The dynamics of the pre-transition stage is exhibited in figure 7(*b*), where VF manifests a decrease in magnitude at the viscous sublayer, and even undershoots its final steady-state within this region. It is interesting to note that during this period, VF is still growing in magnitude and propagating radially at the buffer region. Indeed, within the buffer region, the magnitude of VF at the end of the pre-transition stage overshoots the final steady-state at a higher Reynolds number, which implies that during the pre-transition stage, VF works as an increasing momentum sink at the buffer. In the same figure, TI shows a progressive increment in magnitude that occurs first at the viscous sublayer and, subsequently, its peak, located in the buffer, moves further from the wall. This increase in the turbulent force, particularly within the viscous and buffer layers, is a result of the energy growth observed in the stretched vortices and elongated streaks that characterise the pre-transition stage.

The transition stage, depicted in figure 7(*c*), exhibits a continuous increment of magnitude, and a shifting in the peak in both VF^{+0} and TI^{+0} towards the wall. This observation suggests that the near-wall region becomes thinner during this stage, and there is a progressive growth in the population of vortical structures within the buffer region. Indeed, during $113 \leqslant t^{+0} \leqslant 171$, it is interesting to note that TI overshoots the final steady-state at $10 < y^{+0} < 30$. This behaviour implies an enhanced turbulence activity at the buffer that propagates towards the viscous sublayer and the outer regions as time progresses.

Figure 7(*d*) shows that after $t^{+0} \gtrsim 300$, the VF term has reached a steady state, as it is almost invariant. This result is consistent with the plateau reached by the friction coefficient observed in figure 2(*b*). However, it is still possible to observe a small reduction in TI at the buffer region and a slight undershoot in the outer layer's turbulent forces compared with the final steady-state. This implies that there still exists a slow momentum re-distribution associated with the turbulent transport from the more productive regions (viscous and buffer) towards the pipe core. The present findings reveal that the small-scale motions, which are more abundant at the near-wall region, respond first, whereas the less intermittent large-scale structures located at the outer layer require larger time scales to regenerate completely towards their final steady-state. The slower response presented by the core of the flow is analysed further in § 3.7.

3.5. *Characteristics of the four stages based on four-layer dynamic behaviour*

The VF/TI has been proven to be an effective method to understand the distribution of momentum along the wall-normal direction in steady turbulent wall-bounded flows (Wei *et al.* 2005). Here, we use this approach to further investigate the physics associated with the redistribution of momentum during the transitional stages of a temporally-accelerated, turbulent pipe flow.

Figure 8(*a*) reveals that during the inertial stage, VF becomes more dominant and propagates in the wall-normal direction up to $y^{+0} \approx 15$, which increases the thickness of layer I momentarily. This effect quickly reduces the width of layer II (where the turbulent and viscous forces balance one another) until it becomes negligible. At $y^{+0} > 20$, the zero-crossing of TI and the outer behaviour of both TI and VF remain unchanged from the initial steady-state (i.e. $t^{+0} = 0$). Consequently, our results provide further evidence that the turbulent eddies remain unchanged during the inertial stage and are advected in the streamwise direction without a noticeable increment in their energy. This implies that there is no increment in TKE production at this stage because no energy has yet been extracted from the mean flow.

Figure 8(*b*) exhibits the time evolution of the momentum distribution during the pre-transition stage. Near the onset of this period ($t^{+0} \approx 18$), the viscous forces are dominant from the wall up to the buffer region. The temporal evolution of the balance during the pre-transition shows that near the wall $y^{+0} < 3$, the high magnitude of VF starts to reduce. However, during $18 \lesssim t^{+0} \lesssim 60$, it is noticed that VF has a leading order from the wall up to the overlap region. This shows that during the pre-transition stage, the four-layer dynamic behaviour that characterises fully-developed turbulent flows does not hold. Nevertheless, the results exhibited in figure 8(*b*) suggest that during pre-transition, a significant momentum redistribution exists, mainly at the near-wall region. This momentum reallocation is related to a quick decay in the magnitude of VF and a progressive energy growth of the velocity streaks.

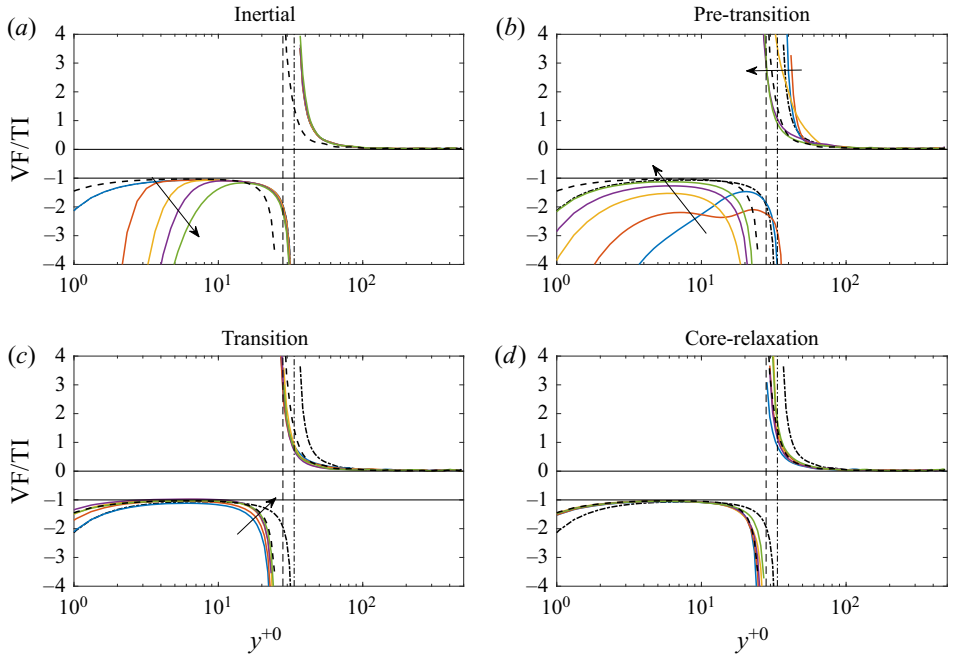

Figure 8. The VF/TI ratio of the four stages experienced for case TP1. The colour legend is the same as that used in figure 5. The arrows represent an increase in time. The vertical lines indicate the location of the zero-crossing of TI, where (– · –) initial turbulent steady-state, (– – –) final steady-state.

By the end of the pre-transition ($t^{+0} \approx 90$), it is possible to observe several fascinating features in the mean momentum distribution. First, layer I has moved back to a similar position compared with the initial steady-state at $y^{+0} \leqslant 3$. Second, we begin to observe a recovery in layer II. A quite interesting characteristic of this stage shows that layer III shifts from its initial position to a location closer to the final steady-state in a relatively short period. Therefore, these results suggest that even though TI and VF are still developing during this stage, both of them change proportionally within layer III. Additionally, during the pre-transition period, the zero-crossing of TI starts moving towards the wall. This implies that the near-wall region starts becoming thinner owing to the increase in Re. From layer IV, associated with the dynamics of the outer region, it is not possible to obtain further details of the flow dynamics because, within this layer, the VF is negligible compared with TI.

During the transition stage, shown in figure 8(*c*), layer I becomes thinner as time increases, which implies a progressive growth in the friction Reynolds number Re_τ and an increment in the population of vortical structures within the inner region. Additionally, at $t^{+0} \approx 171$, layer II becomes temporally thicker than the final steady-state, which shows that the turbulent force develops faster than VF during the transition stage at the near-wall region. In contrast, layer III becomes slightly thinner close to the end of this stage. This behaviour reveals an overshoot in the turbulent forces that occurs first within the viscous sublayer and then propagates towards the buffer region. Therefore, new turbulent structures are principally localized at the viscous sublayer and the buffer region during the transition stage. Although the behaviour in layer IV seems to remain unchanged, the results observed previously in figure 7(*c*) exhibit an undershoot in the response of the turbulent forces in the wake region during this period.

Figure 8(*d*) shows that the VF/TI ratio does not reveal noticeable changes in layers I and II during the core-relaxation stage. However, during this period, a progressive thickening of layer III and a slight narrowing in layer IV are noted. This change in the thickness of layers III and IV indicates that the new turbulence, generated within the buffer, which, during the transitional stage, exceeded the magnitude of TI values at its final steady-state, need to re-distribute towards the outer region. These results also reveal that the horizontal plateau in C_f could be a misleading parameter to identify the onset of the final steady-state, as turbulence energy is still re-distributed at a slow pace in the outer region during the core-relaxation stage. Additionally, the behaviour in the wake region is not captured adequately by the friction coefficient because τ_w and U_b do not present changes during the core-relaxation stage. Moreover, the Reynolds shear stress evolution, shown previously, revealed that it takes a considerable amount of time to reach statistically steady turbulence, and these time scales seem to be *Re*-dependent. Consequently, in the following section, we show that the decomposition of the friction coefficient, in terms of its dynamic contributions, might also be a more suitable approach to understand the momentum redistribution in integral form. This method seems to be satisfactory to determine the onset of the fully-turbulent steady-state.

3.6. *FIK identity for a transient pipe flow*

Fukagata, Iwamoto & Kasagi (2002) developed an exact expression to quantify the different contributions of the flow dynamics into the friction coefficient for canonical wall-bounded flows. This expression is commonly known as the FIK identity, and has been used to provide a meaningful physical decomposition of the wall friction. Our objective is to shed light on the dominant dynamics that contribute to the bypass, transition-like behaviour of C_f during the four transitional stages identified in the previous sections. Consequently, we have derived an expression suitable for an unsteady pipe flow whose dynamics are time-dependent and homogeneous in the streamwise direction, starting from the expression in cylindrical coordinates proposed by Fukagata *et al.* (2002) and shown in (3.2).

$$C_f = \frac{16}{Re_b} + 16\int_0^1 2r\,\langle u_r u_z\rangle\, r\,\mathrm{d}r - 16\int_0^1 (r^2-1)\left(I_z'' + \frac{\mathrm{d}p''}{\mathrm{d}z} + \frac{\mathrm{d}\,\langle U_z\rangle}{\mathrm{d}t}\right) r\,\mathrm{d}r. \tag{3.2}$$

For the unsteady flow problem, it is evident that PG is time-dependent. Hence, it can be computed in terms of the streamwise mean momentum balance (see (3.1)) as

$$\frac{\partial p}{\mathrm{d}z} = \frac{1}{r}\frac{\partial\,(r\tau)}{\partial r} - \frac{\mathrm{d}\,\langle U_z\rangle}{\mathrm{d}t}, \tag{3.3}$$

where $\tau(y,t)$ represents the total shear stress (sum of the viscous and Reynolds shear stresses). The total shear stress τ in the accelerating pipe flow does not have a linear behaviour in the wall-normal direction during the transitional stages, in contrast with steady turbulent flows (see figure 5), and it is time-dependent. Then, the deviation from the mean and the bulk quantity (denoted by the double prime) in PG is given by

$$\frac{\mathrm{d}p''}{\mathrm{d}z} = \frac{1}{r}\frac{\partial\,(r\tau)}{\partial r} - \frac{2}{R}\int_0^1 \frac{1}{r}\frac{\partial\,(r\tau)}{\partial r} r\,\mathrm{d}r - \frac{\mathrm{d}\,\langle U_z\rangle}{\mathrm{d}t}. \tag{3.4}$$

Note that the accelerating flow cases studied here are homogeneous in the streamwise direction; hence, the inhomogeneous term $I_z'' = 0$ (see Kasagi & Fukagata 2006).

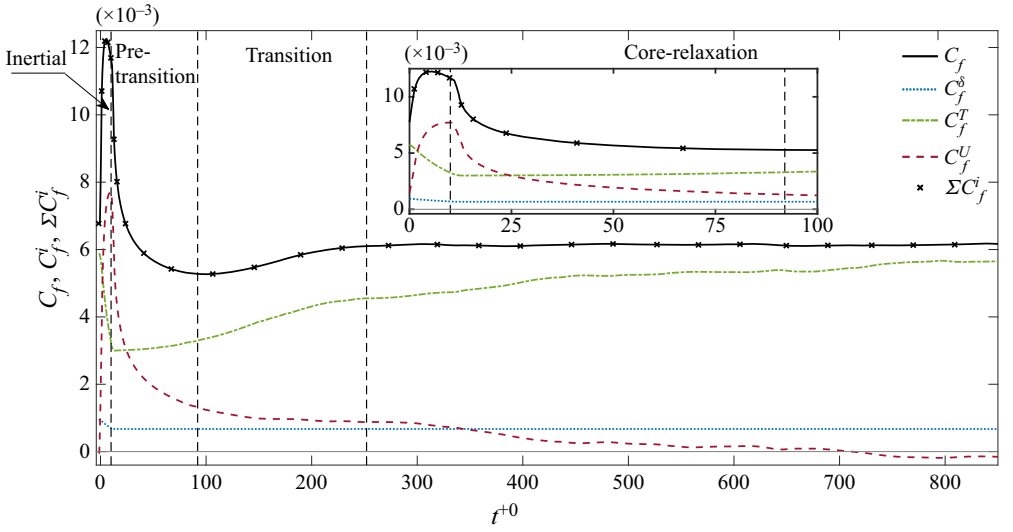

Figure 9. Time dependence of each term of the FIK identity applied in case TP1. (——) Skin friction coefficient C_f, (· · · · · ·) laminar contribution C_f^δ, (— · —) turbulent contribution C_f^T, (— — —) unsteady contribution C_f^U, (×) sum of the three dynamic components ($C_f^\delta + C_f^T + C_f^U$). Note that ΣC_f^i overlaps exactly with C_f. The vertical dashed lines divide the four stages defined in this study. The inset is a zoomed view of the skin friction coefficient and its different contributions during the inertial and pre-transition stages.

The substitution of (3.4) into (3.2) leads to (3.5), which is an FIK identity suitable for temporally-accelerated (unsteady) pipe flows, homogeneous in the streamwise direction.

$$C_f = \underbrace{\frac{16}{Re_b}}_{C_f^\delta} + \underbrace{16\int_0^1 2r\,\langle u_r u_z\rangle\, r\,\mathrm{d}r}_{C_f^T} \underbrace{- 16\int_0^1 (r^2-1)\left(\frac{1}{r}\frac{\partial\,(r\tau)}{\partial r} - \frac{2}{R}\int_0^1 \frac{1}{r}\frac{\partial\,(r\tau)}{\partial r} r\,\mathrm{d}r\right) r\,\mathrm{d}r}_{C_f^U}. \tag{3.5}$$

To ease the analysis of the different contributions to the total friction coefficient, (3.5), throughout this paper, will be represented as

$$C_f = C_f^\delta + C_f^T + C_f^U, \tag{3.6}$$

where C_f^δ and C_f^T represent the laminar and the turbulent contributions, respectively. The substitution of (3.4) into (3.2) cancels the acceleration term and allows examination of the effects of the gradient of the total shear stress ($\tau(y,t)$), which is directly related to the transient behaviour of the flow, as observed from (3.3). Therefore, the term C_f^U represents both the contribution of PG and the unsteady term.

Figure 9 is the result of applying equation (3.5) to the data obtained from case TP1. First, the sum of the different dynamic contributions to the friction coefficient (ΣC_f^i) collapses with the friction coefficient. Consequently, this result gives us confidence with the alternative form of the FIK identity presented in this study.

As expected, before the flow excursion ($t^{+0} \leqslant 0$), the largest contribution to C_f is provided by the turbulent term C_f^T as the simulations initiated from existing fully-developed turbulent fields. During the inertial stage, the unsteady term C_f^U becomes

dominant, owing to the increment in the inertial forces and the pressure gradient required to accelerate the flow. Simultaneously, the contribution of C_f^T is dramatically reduced because the turbulent forces remain almost unchanged, although the flow rate increases quickly during this short period. Interestingly, the end of the inertial stage, characterized previously by the VF/TI ratio, coincides with the peak found in C_f^U. Thus, this gives further support to the robustness in the current definition of the transient stages and could be an unambiguous indicator to properly define the end of the inertial stage and the onset of the pre-transition.

At the beginning of the pre-transition ($10 \lesssim t^{+0} \lesssim 25$), C_f^U is the dominant term. However, its contribution decays exponentially as time progresses. This reveals that the mean velocity profile evolves rapidly in the near-wall region during this stage within a short interval (see figure 5*b*). Hence, an essential redistribution of momentum occurs during the pre-transition period. However, C_f^T, whose contribution decreased quickly during the inertial stage owing to the sudden increase in the bulk velocity U_b, exhibits a slow and gradual increase during the pre-transition, which is related to an energy growth of the velocity streaks in the near-wall region, shown previously in figure 4(*b*). The turbulent component, C_f^T, becomes the dominant term at $t^{+0} \gtrsim 25$, which shows that the turbulent contributions are relevant even at the pre-transition stage. Finally, the end of the pre-transition stage (onset of transition) occurs near the minimum in C_f, where the wall friction starts to recover, owing to the new turbulence generated at the near-wall region. This definition is consistent with the study by He & Seddighi (2015).

During the transition stage, the contribution of C_f^T grows at a faster pace associated with the generation and propagation of new turbulent eddies, owing to the increment in the Reynolds number. At this stage, the Reynolds stress and, as a consequence, the turbulent force mainly increase within the inner region $y^{+0} < 100$ (see figure 7*c*). However, C_f^U reveals that the unsteady contributions continue decaying slowly. This behaviour suggests that the mean velocity profile continues evolving slowly owing to the effects imposed by the turbulent forces that flatten the initial mean velocity profile as a result of the increments in the Reynolds number.

Finally, the core-relaxation stage exhibits a slow increment in the turbulence energy despite the plateau exhibited by C_f. Although the first peak in C_f after the transition is located at $t^{+0} \approx 300$, the turbulent contribution keeps increasing in magnitude as a function of time up to $t^{+0} \approx 780$. The progressive growth in C_f^T during this stage is related to a tardy turbulence response in the wake region of the flow. Conversely, C_f^U, which reached an apparent plateau at the end of the transition stage, undergoes a faster decay after $t^{+0} > 300$, which indicates that the unsteady contributions in the momentum balance of a temporally-accelerated pipe flow require a long period to become negligible.

At $\Delta t^{+0} \approx 710$, C_f^U becomes negative, as $\mathrm{d}\langle U_z \rangle / \mathrm{d}t \approx 0$ and the pressure gradient $(\mathrm{d}p/\mathrm{d}z)$, which has a negative value, becomes dominant in C_f^U (refer back to (3.3)–(3.6)). Therefore, when C_f^U reaches a negative constant value, it only accounts for the contributions of the pressure gradient, as the final turbulent flow has become completely established. The present results reveal that the end of the core-relaxation stage (the onset of the fully-turbulent steady-state) occurs when C_f^U attains a constant negative value and there exists a plateau in C_f^T (i.e. $\mathrm{d}C_f^T/\mathrm{d}t = 0$). This suggests that the dynamic components of C_f might be more accurate in determining the onset of the steady state rather than the plateau exhibited by C_f after the transitional period. This slow reconstitution in the wake

was observed in the experimental study by Greenblatt & Moss (2004), who were unable to conclude why this region presents such a slow development.

3.7. *Delay in the response of the core region*

From the delayed regeneration of turbulence observed in the wake region, the puzzling question arises as to why it takes such a long time to complete the reconstitution of the wake before the flow reaches its final steady-state. Here we will discuss two highly plausible mechanisms that could explain this phenomenon. First, this lag could be attributed, in part, to the radial propagation of turbulence in accelerating pipe flows. However, it does not fully explain why the core-relaxation stage takes more time than the other transitional stages or the ramp-rise time. The other possible mechanism associated with the slow regeneration of the wake could be the relatively new conceptual view of turbulent internal flows known as the 'quiescent core' (Kwon *et al.* 2014).

By using the method proposed by Adrian *et al.* (2000) to identify UMZs, Kwon *et al.* (2014) identified a large UMZ located at the central region of a channel flow whose turbulent intermittency is low when compared with the rest of the flow. As a result, this region was called the 'quiescent core'. This zone is a large-scale structure of high velocity, which oscillates with the large wavelengths of the flow and is characterized by having abrupt changes (large gradients) on the local velocity profile (Kwon *et al.* 2014). Consequently, a thin viscous shear layer at the boundary of this region exists. Intense vortical structures lie at the edges of this UMZ (de Silva, Hutchins & Marusic 2016); hence, momentum transport and fluid entrainment occur by mechanisms similar to the turbulent/non-turbulent interface found in boundary layers (da Silva, dos Reis & Pereira 2011; Yang, Hwang & Sung 2019).

A brief analysis of the quiescent core of the present accelerating flow cases is exhibited here in that context. The probability distribution function (p.d.f.) of the volumetric streamwise velocity fields normalised by the centreline velocity (U_{CL}) has been computed in figure 10 at the four transitional stages. This approach helps us to determine a suitable threshold to identify the envelope of the core. Based on the results displayed in figure 10, a threshold $U_z/U_{CL} = 0.92$ (dashed vertical line) has been selected as the envelope value for the quiescent core during all the transitional stages. This threshold is consistent with the results presented in previous studies for steady turbulent channel (Kwon *et al.* 2014) and pipe flows (Yang *et al.* 2019). The p.d.f. of the full U_z/U_{CL} volumetric fields reveals how momentum is re-distributed in the different transitional stages.

In figure 10(*a*), during the inertial stage, it is observed that the probability of occurrence of events where $0.5 \lesssim U_z/U_{CL} \lesssim 0.8$ is significantly reduced. In contrast, a significant increment in events where $U_z/U_{CL} > 0.8$ is observed, which implies a noticeable growth in the core region at this early stage. These findings are consistent with the superposition of a developing laminar boundary layer with the initial turbulent flow (Kurokawa & Morikawa 1986; He & Seddighi 2015; Mathur *et al.* 2018). During the pre-transitional stage (figure 10*b*), a small growth of events where $U_z/U_{CL} > 0.92$ and a slight reduction at $0.5 \lesssim U_z/U_{CL} \lesssim 0.8$ are observed. Although the time variation in the probability distribution of the normalised streamwise velocity during the second stage is hardly noticeable, a sudden momentum redistribution in the core region can be observed at the end of this stage (green line). This is consistent with the quick response observed in the Reynolds shear stress at $y^{+0} \approx 200$. As expected, during the transition period (figure 10*c*), there exists a significant momentum redistribution. However, this redistribution occurs mostly outside the core envelope as the probability distribution in the zone where

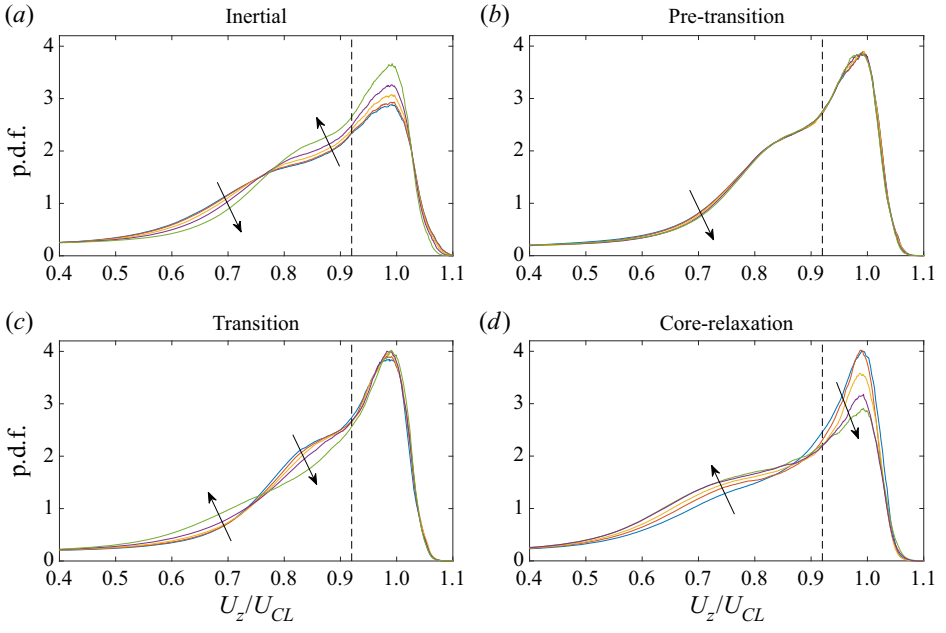

Figure 10. Probability distribution function of the full velocity fields during the four transitional stages studied in the previous sections. The vertical dashed lines at $U_z/U_{CL} = 0.92$ show the threshold used to define the core of the flow, and the arrows indicate increasing time.

$U_z/U_{CL} > 0.92$ exhibits little changes. Growth of events with values $0.5 \lesssim U_z/U_{CL} \lesssim 0.75$ and a decay in the occurrence of events in the range $U_z/U_{CL} \approx 0.75$–0.92 are observed during the transitional period. Finally, the last stage, core relaxation, shows a slow but progressive increment in U_z/U_{CL}, ranging from 0.5 to 0.85, and a more drastic reduction in the occurrence of $0.9 \lesssim U_z/U_{CL} \lesssim 1$ (i.e. within the core envelope). This implies that, during the core relaxation, there exists an exchange of momentum between the flow located within the wake and the overlap region until fully-developed turbulence is reached.

The space–time correlation of the core of the flow has been computed, using the streamwise velocity field as a reference point at $t^{+0} = 356$, where $\Delta\theta$ and Δz represent the spatial shift in the azimuthal and streamwise directions, respectively. These statistics provide an insight regarding the convection velocity of the core and its temporal evolution, relative to the chosen reference point. To compute the cross-correlation of the core, the regions of $U_z/U_{CL} \geqslant 0.92$ at $y/R \approx 0.6$ are correlated. In figure 11(*a–d*), the peak of the correlation (red contour) reveals that the core of the flow advects at a constant velocity, without significant evolution in its enveloping geometry, as though it were an independent plug flow. A similar conclusion is obtained when examining the consecutive snapshots of the core displayed in figure 11(*e*,*h*). The four snapshots presented here have been taken for a total timespan $\Delta t^{+0} \approx 72$ (i.e. the time intervals between each snapshot is $\Delta t^{+} \approx 24$), where the core of the flow convects without displaying a significant evolution in its shape. The correlation also reveals that the core of the flow structure moves on a straight line over $\Delta\theta = 0$, which suggests that this quiescent structure does not rotate, even though it exhibits a somewhat spiral shape. It should be mentioned that similar behaviour was educed from the temporal dependency of the Reynolds stress tensor in pulsating flows at high driving frequencies (Scotti & Piomelli 2001).

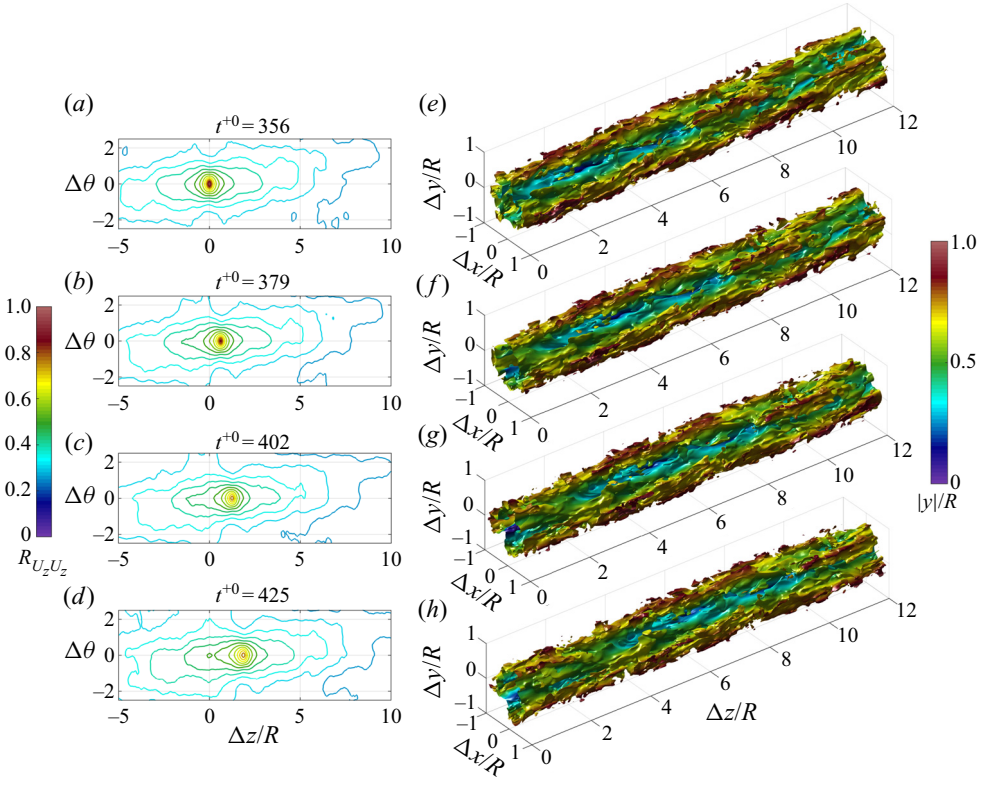

Figure 11. Evolution of the core in a time span $\Delta t^{+0} \approx 72$. (*a–d*) Contours of the two-dimensional cross correlation of streamwise velocity ($R_{U_zU_z}$) during the core-relaxation stage at $y/R \approx 0.6$ in time intervals $\Delta t^{+0} = 24$. (*e–h*) Isosurface of the core envelope computed at $U_z/U_{CL} = 0.92$ for the same consecutive flow realisations used in panels (*a–d*). Note that although the cross correlation has been computed using the complete flow realisations, the core envelope observed in (*e–h*) is displayed over a domain length $12R$ for clarity.

Figure 12 displays the magnitude of the peaks obtained from the cross-correlations computed for a longer period for the transition and core-relaxation stages. The results show that the core envelope maintains a geometric coherence over extensive time intervals during both stages. During the transitional stage, the core evolves at a slower pace compared with the relaxation stage. This is consistent with the previous sections' results and implies that the 'new' turbulence generated at $y^{+0} \lesssim 50$ has little influence on the wake during the transitional period. In contrast, the correlation of the core envelope during the last stage undergoes a faster decay as the turbulent eddies generate an exchange of momentum between the inner and outer regions of the flow. As a result, the passive behaviour of the core region and a slow but progressive radial propagation of turbulence at the wake answers the question posed by Greenblatt & Moss (2004) regarding the large volumes of time required to see a core reconstitution in accelerating turbulent flows effectively. During the core-relaxation stage, the time scales required to reconstitute the core of the flow are considerably larger than the first three stages, and it is expected that there will be a *Re* dependence of this stage as the near-wall region becomes narrower with increasing Reynolds numbers.

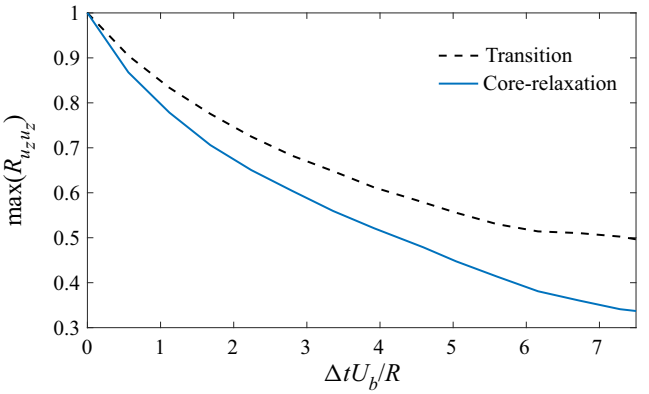

Figure 12. Temporal dependency of the peaks of the space–time correlation $R_{U_z U_z}$ over a time domain $0 \leqslant \Delta t U_b/R \leqslant 7.5$ ($0 \leqslant \Delta t^{+0} \lesssim 165$).

4. Summary and conclusions

The present investigation has characterised the different stages experienced by a turbulent pipe flow during and after it has been temporally accelerated, following a quick ramp-up increment in its flow rate. Compared with previous works that provide a very detailed picture of the kinematics of motion of accelerating wall-bounded internal flows (He & Jackson 2000; He & Seddighi 2013), the present investigation unravels in detail the temporal evolution of the flow dynamics and momentum redistribution processes during the transient process between two steady turbulent Reynolds numbers, using different approaches. The results found in this paper consolidate and extend previous investigations (Maruyama *et al.* 1976; He & Jackson 2000; Greenblatt & Moss 2004; He & Seddighi 2013, 2015) and show that the transient behaviour of a pipe flow during and after a rapid temporal acceleration follows four stages: inertial, pre-transition, transition and core relaxation. Finally, the slow regeneration in the wake region, namely core relaxation, is investigated in terms of a recent conceptual view of internal wall-bounded turbulent flows called the 'quiescent core'. Based on the different approaches used in this study, the four transient stages exhibit different and unambiguous flow features, listed as follows.

(i) The inertial stage, which triggers the transient behaviour of the initially turbulent flow, manifests a frozen turbulence response. This is noticed in the behaviour of the turbulent eddies, which advect with the mean flow without undergoing deformation. These observations are supported by the invariant behaviour of the Reynolds shear stress during this period. Simultaneously, the viscous shear stress exhibits a rapid increase in magnitude as the flow is accelerated. This considerable increment in the viscous shear stress occurs mainly within the viscous sublayer and is generated by the superposition of a plug-like inflow owing to the increase in the flow rate. Subsequently, the viscous shear propagates towards the buffer region. From a dynamic point of view, the VF (gradient of the viscous shear stress) grows in magnitude in the near-wall region and becomes a significant momentum sink, as the flow-rate increases, to preserve the no-slip condition. Consequently, the VF/TI ratio shows a widening of layer I and a narrowing in layer II, until the latter becomes negligible. Therefore, as the flow is accelerated, our results suggest that a layer strongly dominated by the viscous forces extending from the wall up to $y^{+0} \approx 10$ is formed temporally.

(ii) At the beginning of the pre-transition stage, a weak response of the turbulent inertia is observed near the wall, within $3 < y^{+0} < 15$. As time progresses, TI shows a gradual increment, only at the near-wall region, and its peak seems to be shifted away from the wall, which explains the relocation of the peak of TKE production at this stage. In contrast, the high magnitude of VF, reached during the inertial stage, decays at the viscous sublayer and propagates towards the buffer region. This reduction in the magnitude of VF at the wall is reflected as a progressive recovery of layers I and II in the VF/TI ratio. Consequently, by the end of the pre-transition stage, it is revealed that the forces at $y^{+0} < 10$ exhibit a balance proportional to the initial steady-state. The end of the pre-transition (onset of transition) is marked by the minimum magnitude reached by the viscous forces at the viscous sublayer, which nominally coincides with the minimum temporal value in C_f, as suggested by He & Seddighi (2015).

The instantaneous flow visualisations reveal that during the pre-transition, the near-wall vortical structures are stretched, owing to the formation of thin layers of high strain as the flow is accelerated. As a result, streamwise vortex filaments are created. These streamwise swirls are associated with the elongation and energy growth of the streaks observed in previous studies (He & Seddighi 2013).

(iii) The transition stage is characterised by rapid growth in the magnitude of TI and VF at the near-wall region. During this period, the turbulent forces near the wall develop slightly faster than the viscous forces. The same conclusion is obtained by analysing the turbulent and the unsteady contributions of C_f during this stage, by using an FIK identity applicable for unsteady flows. The recovery in VF and C_f during the transition stage is a consequence of higher population and propagation of turbulent eddies within the buffer layer.

The end of the transition period is characterised by a quasi-steady-state of TI and VF at the inner region ($y^{+0} \lesssim 50$) and a plateau reached by the friction coefficient. Nevertheless, the wake region is not fully reconstituted at the end of this stage. These results are consistent with Greenblatt & Moss (2004) and He & Seddighi (2013), who observed a slow response in turbulence at the wake region of accelerating pipe and channel flows, respectively.

(iv) The core-relaxation stage is associated with a delayed turbulence response at the outer region of the flow ($y^{+0} \gtrsim 50$). This is observed in the very slow reconstitution of the Reynolds shear stress at the outer region, even when the near-wall region has reached a quasi-steady-state. By analysing the different dynamic contributions to C_f in terms of the FIK identity, the present study reveals that progressive growth in the turbulent contribution C_f^T exists during the core-relaxation period together with a proportional decay in the unsteady term C_f^U. Consequently, it is revealed that for accelerating turbulent flows starting at moderate Re, the plateau reached by the turbulent and the unsteady contributions to C_f might be a suitable indicator to show that the flow has reached the final steady-state.

Finally, a brief examination of the core region has been conducted to further understand the structural behaviour of the core of the flow (the largest UMZ of the flow), computed as the region enveloped by a surface where $U_z = 0.92U_{CL}$. Interestingly, our results show that not only the radial propagation of turbulence but also the recent conceptual view of the core region of the flow, the 'quiescent core' (Kwon *et al.* 2014; Yang *et al.* 2019), contribute to this behaviour. Also, the two-dimensional cross-correlation of the streamwise velocity at $y/R \approx 0.6$ shows that the core region convects in the axial direction and requires a large

time interval ($tU_b/R > 7$) to present a substantial evolution. Consequently, this answers the question posed by Greenblatt & Moss (2004), who also observed a slow reconstitution of the core region of accelerating pipe flows.

Funding. This work was supported with supercomputing resources provided by the Phoenix HPC service at the University of Adelaide. This research was also undertaken with the assistance of resources provided at the NCI NF through the Computational Merit Allocation Scheme, supported by the Australian Government and the Pawsey Supercomputing Centre, with funding from the Australian Government and the Government of Western Australia. The authors acknowledge the financial support of the Australian Research Council.

Declaration of interests. The authors report no conflict of interest.

Author ORCIDs.
Byron Guerrero https://orcid.org/0000-0001-7890-6265;
Martin F. Lambert https://orcid.org/0000-0001-8272-6697;
Rey C. Chin https://orcid.org/0000-0002-2709-4321.

References

Adrian, R., Meinhart, C. & Tomkins, C. 2000 Vortex organization in the outer region of the turbulent boundary layer. *J. Fluid Mech.* **422**, 1–54.

Annus, I. & Koppel, T. 2011 Transition to turbulence in accelerating pipe flow. *Trans. ASME J. Fluids Engng* **133**, 071202.

Avila, K., Moxey, D., de Lozar, A., Avila, M., Barkley, D. & Hof, B. 2011 The onset of turbulence in pipe flow. *Science* **333** (6039), 192–196.

Chin, C. 2011 Numerical study of internal wall-bounded turbulent flows. PhD thesis, The University of Melbourne.

Chin, C., Philip, J., Klewicki, J., Ooi, A. & Marusic, I. 2014 Reynolds-number-dependent turbulent inertia and onset of log region in turbulent pipe flows. *J. Fluid Mech.* **757**, 747–769.

Dey, S. & Lambert, M.F. 2005 Reynolds stress and bed shear in nonuniform unsteady open-channel flow. *J. Hydraul. Engng ASCE* **131**, 610–614.

Fischer, P., Lottes, J. & Kerkemeier, S. 2019 Nek5000, Web page https://nek5000.mcs.anl.gov.

Fukagata, K., Iwamoto, K. & Kasagi, N. 2002 Contribution of Reynolds stress distribution to the skin friction in wall-bounded flows. *Phys. Fluids* **14**, L73–L76.

Greenblatt, D. & Moss, E. 1999 Pipe-flow relaminarization by temporal acceleration. *Phys. Fluids* **11**, 3478.

Greenblatt, D. & Moss, E. 2004 Rapid temporal acceleration of a turbulent pipe flow. *J. Fluid Mech.* **514**, 65–75.

Guerrero, B., Lambert, M.F. & Chin, R.C. 2020 Extreme wall shear stress envents in turbulent pipe flows: spatial characteristics of coherent motions. *J. Fluid Mech.* **904**, A18.

He, K., Seddighi, M. & He, S. 2016 DNS study of a pipe flow following a step increase in flow rate. *Intl J. Heat Fluid Flow* **57**, 130–141.

He, S., Ariyaratne, C. & Vardy, A.E. 2011 Wall shear stress in accelerating turbulent pipe flow. *J. Fluid Mech.* **685**, 440–460.

He, S. & Jackson, J.D. 2000 A study of turbulence under conditions of transient flow in a pipe. *J. Fluid Mech.* **408**, 1–38.

He, S. & Seddighi, M. 2013 Turbulence in transient channel flow. *J. Fluid Mech.* **715**, 60–102.

He, S. & Seddighi, M. 2015 Transition of transient channel flow after a change in Reynolds number. *J. Fluid Mech.* **764**, 395–427.

Head, M.R. & Bandyopadhyay, P. 1981 New aspects of turbulent boundary-layer structure. *J. Fluid Mech.* **107**, 297–338.

Hof, B., de Lozar, A., Avila, M., Tu, X. & Schneider, T. 2010 Eliminating turbulence in spatially intermittent flows. *Science* **327** (5972), 1491–1494.

Jeong, J. & Hussain, F. 1995 On the identification of a vortex. *J. Fluid Mech.* **285**, 69–94.

Jung, S. & Chung, Y. 2012 Large-eddy simulation of accelerated turbulent flow in a circular pipe. *Intl J. Heat Fluid Flow* **33**, 1–8.

Jung, S. & Kim, K. 2017 Transient behaviors of wall turbulence in temporally accelerating channel flows. *Intl J. Heat Fluid Flow* **67**, 13–26.

KASAGI, N. & FUKAGATA, K. 2006 *The FIK Identity and its Implication for Turbulent Skin Friction Control*, chap. 10, pp. 297–324. World Scientific Publishing.

KLEWICKI, J., CHIN, C., BLACKBURN, H.M., OOI, A. & MARUSIC, I. 2012 Emergence of the four layer dynamical regime in turbulent pipe flow. *Phys. Fluids* **24**, 045107.

KUROKAWA, J. & MORIKAWA, M. 1986 Accelerated and decelerated flows in a circular pipe. *Bull. JSME* **29**, 758–765.

KWON, Y.S., PHILIP, J., DE SILVA, C.M., HUTCHINS, N. & MONTY, J.P. 2014 The quiescent core of turbulent channel flow. *J. Fluid Mech.* **751**, 225–254.

MARUYAMA, T., KURIBAYASHI, T. & MIZUSHINA, T. 1976 The structure of the turbulence in transient pipe flows. *J. Chem. Engng Japan* **9**, 431–439.

MATHUR, A. 2016 Study of accelerating and decelerating turbulent flows in a channel. PhD thesis, The University of Sheffield.

MATHUR, A., GORJI, S., HE, S., SEDDIGHI, M., VARDY, A.E., O'DONOGHUE, T. & POKRAJAC, D. 2018 Temporal acceleration of a turbulent channel flow. *J. Fluid Mech.* **835**, 471–490.

PERRY, A.E. & CHONG, M.S. 1982 On the mechanism of wall turbulence. *J. Fluid Mech.* **119**, 173–217.

SCOTTI, A. & PIOMELLI, U. 2001 Numerical simulation of pulsating turbulent channel flow. *Phys. Fluids* **13**, 1367.

SEDDIGHI, M., HE, S., VARDY, A.E. & ORLANDI, P. 2013 Direct numerical simulation of an accelerating channel flow. *Flow Turbul. Combust.* **92**, 473–502.

DE SILVA, C., HUTCHINS, N. & MARUSIC, I. 2016 Uniform momentum zones in turbulent boundary layers. *J. Fluid Mech.* **786**, 309–331.

DA SILVA, C., DOS REIS, R. & PEREIRA, J. 2011 The intense vorticity structures near the turbulent/non-turbulent interface in a jet. *J. Fluid Mech.* **685**, 165–190.

SUNDSTROM, L. & CERVANTES, M. 2017 The self-similarity of wall-bounded temporally accelerating turbulent flows. *J. Turbul.* **19**, 49–60.

VARDY, A. & BROWN, J. 2003 Transient turbulent friction in smooth pipe flows. *J. Sound Vib.* **259**, 1011–1036.

VARDY, A., BROWN, J., HE, S., ARIYARATNE, C. & GORJI, S. 2015 Applicability of frozen-viscosity models of unsteady wall shear stress. *J. Hydraul. Engng ASCE* **141**, 04014064.

WEI, T., FIFE, P., KLEWICKI, J. & MCMURTRY, P. 2005 Properties of the mean momentum balance in turbulent boundary layer, pipe and channel flows. *J. Fluid Mech.* **522**, 303–327.

WU, X., MOIN, P., ADRIAN, R.J. & BALTZER, J.R. 2015 Osborne Reynolds pipe flow: direct simulation from laminar through gradual transition to fully developed turbulence. *Proc. Natl Acad. Sci. USA* **112**, 7920–7924.

YANG, J., HWANG, J. & SUNG, H. 2019 Influence of wall-attached structures on the boundary of the quiescent core region in turbulent pipe flow. *Phys. Rev. Fluids* **4**, 114606.